Theor Chem Acc (2007) 117:915–931
DOI 10.1007/s00214-006-0210-5

REGULAR ARTICLE

Electron-transfer in molecular functional materials

Anna Painelli · Francesca Terenziani · Zoltán G. Soos

Received: 20 June 2006 / Accepted: 13 October 2006 / Published online: 22 December 2006
© Springer-Verlag 2006

Abstract We discuss electron-transfer processes that govern the physics of several materials or systems of interest for advanced applications. The discussion touches upon several topics, ranging from solvatochromism to solvent-induced symmetry breaking, from excitonic to cooperative effects in molecular crystals, from phase transitions to vibrational contributions to the dielectric constant in organic materials, from spectroscopy to molecular transport. In all these diverse systems electron transfer (ET) plays a major role and is discussed with reference to simple models for delocalized charges.

Keywords Electron transfer · Non-linear optics · Molecular transport · Molecular junctions · Polarization and polarizability · Charge-transfer salts · Organic chromophores · Solvatochromism · Absorption and fluorescence spectroscopy

1 Introduction

Electron-transfer (ET) is a fundamental process in chemistry and biology and is the key process in organic electronics in its wide context. Understanding molecular junctions, photoconversion devices, organic light-emitting devices, just as an example, requires a thorough understanding of ET. ET describes the motion of an electron between different sides of the same molecule (intramolecular ET) or between different molecules (intermolecular ET). In either case an electric charge moves along a sizeable distance: ET processes generate large electric fields and are strongly affected by electric fields. This simple consideration explains why materials with delocalized electrons, i.e. materials where ET plays a basic role, are so interesting for non-linear optics (NLO): an applied electric field in fact displaces delocalized electrons leading to large response fields and hence to non-linear behavior. Electric fields need not to be applied from the outside: large fields can be experienced by electrons inside a material as due to their interaction with surrounding charges. These *environmental* electric fields affect the ET process in the material, leading to important phenomena.

Here we discuss ET processes occurring in several materials of interest for advanced applications. In the next section intramolecular ET is investigated in so called quadrupolar chromophores, a class of π-conjugated molecules with two donor (D) groups joined by π-bridge to a central acceptor (A) core leading to linear centrosymmetric DAD structures (of course the discussion also applies to ADA structures). These molecules, widely studied for two-photon absorption (TPA) applications, are characterized by a fairly complex spectroscopic behavior [1,2]. Here we discuss how the interaction between ET and vibrational and/or solvation degrees of freedom can induce symmetry breaking in the ground or excited state, and ascribe the unusual spectroscopic behavior of these dyes in solution to this phenomenon.

In the third section we discuss the role of intermolecular electrostatic interactions in clusters of polar DA chromophores. These molecules, also called push–pull

A. Painelli (✉) · F. Terenziani
Dip. Chimica GIAF, Parma University& INSTM UdR Parma, 43100 Parma, Italy
e-mail: anna.painelli@unipr.it

Z. G. Soos
Department of Chemistry, Princeton University, Princeton, NJ 08544, USA

chromophores, are an interesting class of molecules with applications in molecular photonics and electronics [3]. In aggregates, films or crystals, push-pull chromophores pack with negligible intermolecular overlap, but electrostatic intermolecular interactions are strong. The intramolecular ET process occurring at different locations amplifies the effects of intermolecular electrostatic interactions, so that the motion of an electron in a molecule actually affects ET processes at nearby (and not so nearby) molecules. Resulting collective and cooperative effects dominate the physics of these systems that represent interesting model systems to investigate the role of classical electrostatic interactions on intramolecular ET.

In the fourth section we will discuss charge-transfer (CT) crystals with a mixed stack motif [4]. In these materials electron donors such as tetrathiafulvalene (TTF) and electron acceptors such as chloranil (CA) alternate to form one-dimensional (1D) stacks. The frontier orbitals on adjacent molecules overlap significantly as testified by the fractional average ionicity on the molecular sites. Much as with push–pull or quadrupolar chromophores, the low-energy physics of these materials is governed by ET. But in CT salts ET is intermolecular and leads to delocalized electrons in the stack direction. Charge and lattice instabilities dominate the physics of these materials and require fairly complex models accounting for delocalized electrons in 1D, electrostatic interactions in 3D and electron–phonon coupling.

Section 5 shortly summarizes a recent view of electron transport in molecular junctions. ET represents of course the basic process in molecular transport, but in a molecular junction we want a continuous flux of electrical charge that holds for a long (infinite) time. In other terms, molecular junctions are driven systems and work in non-equilibrium steady state conditions [5]. We will present a simple approach to the problem based on a real-space description of the junction, that lead to a chemically appealing view of the molecule as an electrical circuit with the current flowing through chemical bonds.

2 Environmental effects on ET systems: solvent induced symmetry breaking in quadrupolar (DAD) chromophores

Intramolecular ET dominates the low-energy physics of dipolar (DA), quadrupolar (DAD) or multipolar (AD_n) chromophores for NLO applications. In these systems an electron-acceptor (A) is linked to one or more electron-donor (D) groups (of course the D and A may be exchanged leading to structures like ADA or DA_n). Charge-resonance few-state models have been successfully applied to describe these systems: their electronic structure, as far as low-energy properties are concerned, can in fact be described based on few electronic states that correspond to the main resonating structures of the chromophore. The prototypical model for the polar DA chromophore is the famous two state model by Mulliken [6,7]. This model, extended to account for the coupling of electronic and vibrational degrees of freedom, has been successfully applied to describe linear and non-linear optical responses of this class of chromophores [8,9]. A further extension to account for the interaction with polar solvents allowed a detailed study of the solvent-dependence of electronic and vibrational spectra [10,11].

Quadrupolar and multipolar chromophores have no permanent dipole moments, neither in the ground nor in the excited states, and, on this basis, one would expect negligible spectroscopic effects of the solvent polarity. However, several chromophores show a strongly solvatochromic fluorescence [2,13–15], a phenomenon that has not been fully understood, so far. Here we focus on quadrupolar DAD chromophores and, based on a charge-resonance model, demonstrate that electron-vibration coupling and/or polar-solvation can induce symmetry breaking in either the excited or the ground state of DAD chromophores, leading to unusual spectroscopic behavior [12].

In the spirit of the Mulliken model [6,7], the charge resonance model for quadrupolar chromophores is written on the basis of three orthogonal states: $|N\rangle$, the neutral state, corresponding to the DAD structure, and two degenerate states, $|Z_1\rangle$ and $|Z_2\rangle$, corresponding to the two zwitterionic structures D^+A^-D and DA^-D^+, respectively. We define 2η as the energy difference between the two degenerate zwitterionic states and the neutral state, so that for positive η the neutral form is lower in energy than the zwitterionic forms, whereas the opposite occurs for negative η. The mixing between the states is described by an off-diagonal matrix element in the Hamiltonian, $\langle N|H|Z_1\rangle = \langle N|H|Z_2\rangle = -\sqrt{2}t$, that measures the probability of electron transfer from D to A and backwards. The two zwitterionic states have large dipole moments, μ_0, pointing in opposite directions. This is by far the largest matrix element of the dipole moment operator in the chosen basis: all other matrix elements of the dipole moment operator will be disregarded.

By exploiting inversion symmetry, we combine the zwitterionic states in symmetric and antisymmetric wavefunctions: $|Z_+\rangle = (|Z_1\rangle + |Z_2\rangle)\Big/\sqrt{2}$ and $|Z_-\rangle = (|Z_1\rangle - |Z_2\rangle)\Big/\sqrt{2}$, respectively. The N state is even, so that it only mixes to $|Z_+\rangle$. On the symmetrized basis, the following three operators are conveniently defined:

$$\hat{\rho} = |Z_+\rangle\langle Z_+| + |Z_-\rangle\langle Z_-|$$
$$\hat{\delta} = |Z_+\rangle\langle Z_-| + |Z_-\rangle\langle Z_+| \quad (1)$$
$$\hat{\sigma} = |Z_+\rangle\langle N| + |N\rangle\langle Z_+|$$

where $\hat{\sigma}$ mixes the two *gerade* states, and the two operators $\hat{\rho}$ and $\hat{\delta}$ define the charge distribution in the molecule: $\hat{\rho} = \hat{\rho}_1 + \hat{\rho}_2$ is the average charge on the central A site, sum of the charges on the two external D sites; $\hat{\delta} = \hat{\rho}_1 - \hat{\rho}_2$ instead measures the charge unbalance on the two external (D) sites. In terms of these operators, the representative matrices of the Hamiltonian and dipole moment operators are

$$H_{el} = 2\eta\hat{\rho} - 2t\hat{\sigma}; \quad \hat{\mu} = \mu_0\hat{\delta}. \quad (2)$$

The eigenstates of the Hamiltonian are

$$|g\rangle = \sqrt{1-\rho}\,|N\rangle + \sqrt{\rho}\,|Z_+\rangle$$
$$|a\rangle = |Z_-\rangle \quad (3)$$
$$|e\rangle = \sqrt{\rho}\,|N\rangle - \sqrt{1-\rho}\,|Z_+\rangle$$

where ρ is the ground state expectation value of $\hat{\rho}$. Its value is fixed by the model parameters, as follows:

$$\rho = 0.5\left(1 - \eta \Big/ \sqrt{\eta^2 + 4t^2}\right) \quad (4)$$

The charge distribution in the ground state can be represented as $D^{+0.5\rho}A^{-\rho}D^{+0.5\rho}$, so that ρ measures the fractional charge on the central A site, i.e. the quadrupolar moment in the ground state. The operator $\hat{\delta}$, proportional to the dipole moment operator, breaks the inversion symmetry and has vanishing expectation values in all states.

Relevant transition energies and dipole moments can be expressed in terms of ρ:

$$\hbar\omega_{ga} = \boldsymbol{\varepsilon}_a - \boldsymbol{\varepsilon}_g = 2t\sqrt{\frac{1-\rho}{\rho}}; \quad \mu_{ga} = \langle g|\,\hat{\mu}\,|a\rangle = \mu_0\sqrt{\rho}$$
$$\hbar\omega_{ge} = \boldsymbol{\varepsilon}_e - \boldsymbol{\varepsilon}_g = 2t\sqrt{\frac{1}{\rho(1-\rho)}}; \quad \mu_{ge} = \langle g|\,\hat{\mu}\,|e\rangle = 0$$
$$\hbar\omega_{ae} = \boldsymbol{\varepsilon}_e - \boldsymbol{\varepsilon}_a = 2t\sqrt{\frac{\rho}{1-\rho}}; \quad \mu_{ae} = \langle a|\,\hat{\mu}\,|e\rangle = \mu_0\sqrt{1-\rho} \quad (5)$$

The odd a state in Eq. (3) is allowed in one-photon absorption (OPA), while the even e state is allowed in two-photon absorption (TPA). For large positive η ($\rho \to 0$) the one- and two-photon excitations become degenerate. In the opposite limit of large and negative η ($\rho \to 1$) the OPA energy goes to zero (the ground state becomes degenerate) whereas the TPA state has a higher energy ($\sim -2\eta$). The other notable case is $\eta = 0$, where $\rho = 0.5$, and the ground, OPA and TPA states are equally spaced in energy.

The coupling between electronic and vibrational degrees of freedom accounts for the different geometry associated with the neutral and zwitterionic states, much as it occurs for polar D-π-A chromophores [7]. The charge rearrangement from N to Z_1 or to Z_2 states occurs along the two different arms of the quadrupolar molecule, so that we introduce two effective coordinates, q_1 and q_2, describing the nuclear motion in each arm. The two coordinates, equivalent by symmetry, have the same harmonic frequency, ω. Introducing the symmetric and antisymmetric coordinates:

$$q_+ = \frac{1}{\sqrt{2}}(q_1 + q_2); \quad q_- = \frac{1}{\sqrt{2}}(q_1 - q_2) \quad (6)$$

and the conjugate momenta, p_+ and p_-, linear electron-vibration coupling is described by

$$H = H_{el} - \sqrt{\varepsilon_v}\omega q_+\hat{\rho} - \sqrt{\varepsilon_v}\omega q_-\hat{\delta} + \frac{1}{2}\left(\omega^2 q_+^2 + p_+^2\right) + \frac{1}{2}\left(\omega^2 q_-^2 + p_-^2\right) \quad (7)$$

where ε_v measures the vibrational relaxation energy, and is related to electron–vibration coupling.

In the adiabatic approximation the vibrational kinetic energy in the above equation is neglected, to define an electronic Hamiltonian that depends on the nuclear coordinates. Since q_- mixes states with different symmetry, the diagonalization of the adiabatic Hamiltonian goes through the diagonalization of a 3 by 3 matrix. The resulting adiabatic eigenvalues, function of q_+ and q_-, define the potential energy surfaces (PES) for the nuclear motion.

Stable eigenstates with respect to symmetry breaking show a single minimum located at $q_- = 0$ and at finite $q_+ = \sqrt{\varepsilon_v}\langle\rho\rangle/\omega$, where $\langle\rho\rangle$ is the expectation value of $\widehat{\rho}$ in the relevant state. Unstable eigenstates instead show a double minimum structure: the symmetrical $q_- = \delta = 0$ solution corresponds to a saddle point and two equivalent minima are found at finite and opposite q_- values ($q_- = \pm\sqrt{\varepsilon_v}\langle\delta\rangle/\omega$), corresponding to two stable states with equal and opposite dipole moment $\pm\mu_0\langle\hat{\delta}\rangle$.

Figure 1 shows the phase diagram for D–π–A–π–A dyes. The stability of the electronic state is defined by the $\left(\partial^2 E/\partial q_-^2\right)_{q_-=0}$: the boundaries in Fig. 1 just mark the points where either the ground or the first excited state curvature changes its sign. Chromophores in the central region (**II** in the figure), have intermediate quadrupolar moment ($\rho \sim 0.3$–0.6), and do not show symmetry breaking in any state: they are truly non polar chromophores. The left region (**I**), describes chromophores with low quadrupolar moment ($\rho <\sim 0.2$): these systems always have a non-dipolar ground state, but the one-photon allowed state, a, is bistable for sufficiently

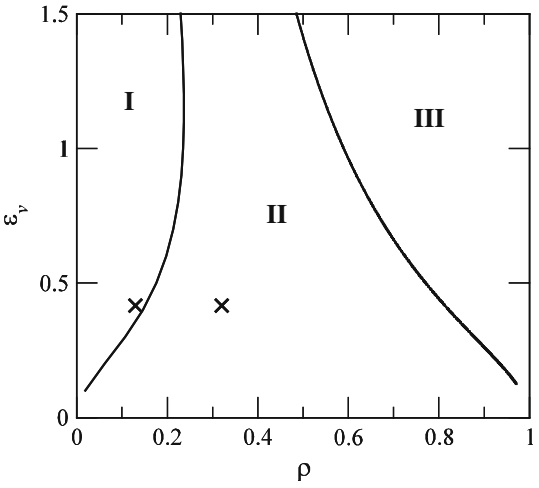

Fig. 1 Phase diagram for quadrupolar chromophores; region **I** corresponds to systems with a stable ground state and bistable OP state; in region **II** all PES have a single minimum; for region **III** the ground state PES has a double minimum. Crosses mark points corresponding to calculation of spectra in Fig. 3. The boundaries represents the lines where the curvature along the q_- coordinate at $q_- = 0$ vanishes for the *g* and *a* states

large ε_v. For class **I** chromophores both the ground state and the TP-allowed state, *e*, are non-dipolar, but the OP-allowed state is bistable and relaxes towards a polar state. In the third region of the phase diagram (**III**), relevant to systems with a large quadrupolar moment ($\rho \rightarrow 1$) and large enough ε_v, both excited states are stable, but the ground state is bistable. This behavior is easily understood: for $\rho \rightarrow 0$ the ground state corresponds to the almost pure *N* state, and the two excited states correspond to Z_- and Z_+. In this limit Z_- and Z_+ are almost degenerate and whatever tiny ε_v induces a symmetry breaking in the excited state. In the $\rho \rightarrow 1$ limit, Z_- and Z_+ are lower in energy than *N*, and the ground state almost coincides with Z_+. The ground state is therefore almost degenerate with the optically allowed state (Z_-) leading to a charge-instability of the ground state itself.

Of course the calculation of a double minimum PES does not guarantee for true symmetry breaking in a finite size system, in fact symmetry can be restored by the fast switching (tunneling) of the system between the two minima [16,17]. Here we concentrate on the calculation of optical spectra and, to avoid any ambiguity about possible false symmetry-breaking in the adiabatic solution, we calculate all spectra from direct diagonalization of the *non-adiabatic* electron-vibration Hamiltonian [9,12,18].

Solvent effects must be accounted for to describe optical spectra in solution [20]. In the spirit of continuum solvation models, and adopting exactly the same approach originally developed for polar DA chromophores [10–12], we account for polar solvation, in the framework of the reaction-field approach. Treating the solvent as an elastic medium, the relevant Hamiltonian reads [10]:

$$H_{\text{solv}} = -\mu_0 F_{\text{R}} \hat{\delta} + \frac{\mu_0^2}{4\varepsilon_{\text{or}}} F_{\text{R}}^2, \tag{8}$$

where F_{R} measures the reaction field, whose equilibrium value is proportional to the solute's dipole moment: $F_{\text{R}}^{(\text{eq})} = \left(2\varepsilon_{\text{or}}/\mu_0^2\right)\left\langle\hat{\mu}\right\rangle$. Here $\langle\hat{\mu}\rangle$ is the expectation value of the dipole moment operator, $\hat{\mu} = \mu_0\hat{\delta}$. The solvent relaxation energy, ε_{or}, measures the energy gained by solvent relaxation in the $N \rightarrow Z_{1/2}$ process. F_{R} couples to the same dipolar operator, $\hat{\delta}$, as the q_- coordinate so that dipolar solvation *cooperates* with vibrational coupling to enforce symmetry breaking and dipolar distortion.

To better understand the role of polar solvation in driving symmetry-breaking, Fig. 2 shows isoenergy lines for the PES relevant to the *a* state of a chromophore of class **I** with $\rho \sim 0.1$ and $\varepsilon_v = 0.4$: even in the non-polar solvent ($\varepsilon_{\text{or}} = 0$, left panel) the PES shows a double minimum. In the presence of polar solvation ($\varepsilon_{\text{or}} > 0$, right panel), three slow (adiabatic) coordinates must be accounted for (q_+, q_- and F_{R}): for graphical reasons we show the isoenergy lines as a function of q_+ and q_-, while keeping F_{R} fixed at its local equilibrium value for the *a* state ($F_{\text{R}} = (2\varepsilon_{\text{or}}/\mu_0)\langle a|\hat{\delta}|a\rangle$). Already in slightly polar solvents (small ε_{or}), a sizeable stabilization of the polar symmetry-broken states is found (of course a second equivalent minimum is found for opposite F_{R} and $\langle a|\hat{\delta}|a\rangle$values), suggesting a strongly solvatochromic fluorescence also in weakly polar solvents.

It is important to realize that the *vertical excited state* always maintains the symmetry of the ground state, so that for class **I** chromophores for which a centrosymmetric ground state is expected, absorption spectra are not affected by polar solvation. On the opposite, steady state fluorescence occurs from the *relaxed excited state*, that for class **I** chromophores is polar: large positive solvatochromism is expected in fluorescence.

The interaction with a dipolar solvent can induce symmetry breaking also in chromophores that in non-polar solvent have stable PES (i.e. in systems where electron–vibration coupling is not strong enough to induce the bistability). Indeed, as far as symmetry breaking is concerned, the total relaxation energy (vibrational + solvation contributions) is the key quantity: only when a threshold value for the total relaxation energy is reached, does symmetry-breaking occur. This implies that for systems with small ε_v, symmetry can be broken only for large ε_{or} values (strongly polar solvents). In this case we

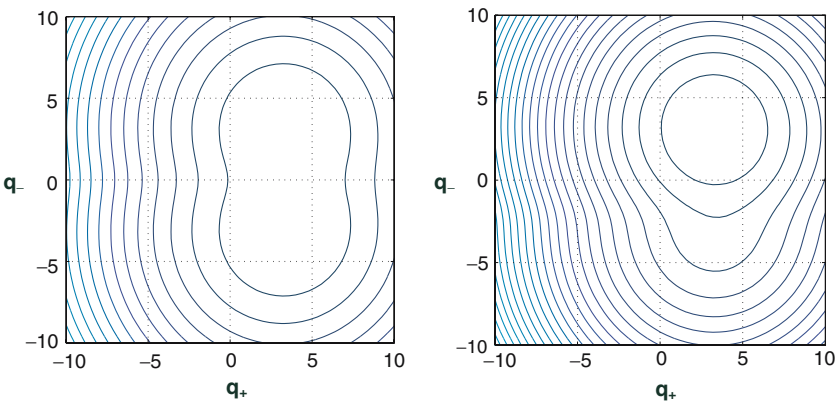

Fig. 2 Isoenergy lines for the *a* state calculated for a chromophore belonging to class **I** for a non-dipolar solvent (*left panel* $\varepsilon_{or} = 0$) and for a polar solvent (*right panel* $\varepsilon_{or} > 0$). In the *right panel* F_R is fixed at its local equilibrium value for the *a* state

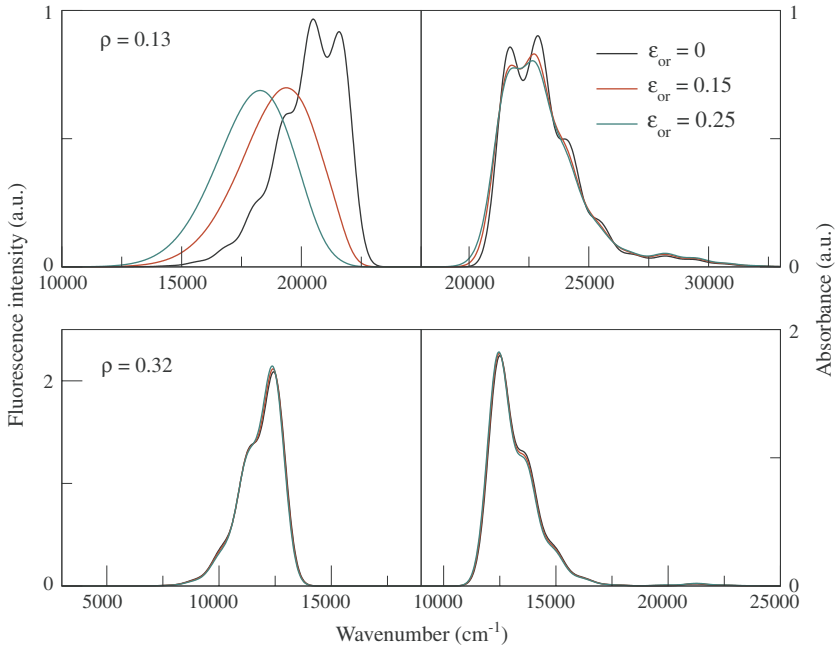

Fig. 3 Fluorescence (*left panels*) and absorption (*right panels*) spectra calculated for systems identified by crosses in Fig. 1. Top panels: **I** region ($\rho = 0.13$, $\sqrt{2}t = 0.8$, $\omega_v = 0.15, \varepsilon_v = 0.25$ eV). Bottom panels: **II** region ($\rho = 0.32$, $\sqrt{2}t = 0.8$, $\omega_v = 0.15, \varepsilon_v = 0.25$ eV). Solvents of increasing polarity are simulated by the ε_{or} parameter (see figure legend, eV)

expect an important fluorescence solvatochromism only for highly polar solvents.

Solvation and vibrational motions have very different time-scales: vibrational coordinates (typically in the mid infrared region) describe a truly quantum mechanical motion, so that, depending on the height of the barrier between the two minima, a fast interconversion (tunneling) between the two symmetry-broken states may restore the original symmetry (the false symmetry-breaking case) [16] . Instead polar salvation involves a very slow (actually overdamped) coordinate, that behaves as a classical coordinate [1] and does not support tunneling. In other words, interconversion between the two symmetry-broken minima is extremely slow in polar solvents since it requires the motion along a slow classical coordinate. Of course spectra in polar solvents must be calculated by summing up the (Boltzmann-weighted) contributions, from the different solute-solvent configurations [10–12].

Chromophores with intermediate ρ (0.25–0.6) are not expected to show any symmetry breaking for realistic values of solvent polarity. For these systems indeed one does not expect any important solvatochromism in either electronic absorption or fluorescence spectra. Figure 3 shows absorption and fluorescence spectra calculated for a class **I** (top panels) and **II** (bottom panels) chromophores, corresponding to the crosses in Fig. 1. The qualitatively different spectroscopic behavior of the two dyes is well apparent. For class **I** chromophores, the effects of symmetry-breaking on fluorescence spectra are shown in the top-left panel, where a strong solvatochromism is predicted, resulting from the dipolar nature of the relaxed excited state. Solvent effects on absorption for the same chromophore (top-right panel) are minor (symmetry is preserved for all states involved in the absorption process) just leading to a solvent induced inhomogeneous broadening. Bottom panels in Fig. 3 show electronic spectra calculated for a class **II**

chromophore that does not undergo symmetry breaking in any solvent: no solvatochromism is observed, since no dipolar states are formed and inhomogeneous broadening itself is ineffective. No examples are shown of spectra for class **III** chromophores: indeed electronic transitions are located for this class of molecules at very low frequencies, down to the IR region, due to the quasi degeneracy of the *g* and *a* states. To the best of our knowledge there are no experimental examples of class **III** DAD chromophores. This may be related to the instability of the ground state towards charge-disproportionation, that most probably reflects in a chemical instability of the compound.

While class **III** systems are missing, several examples are reported in the literature of quadrupolar chromophores with an important fluorescence solvatochromism, that can therefore be classified as class **I** [2,13,15,22,23]. Just as an example, we discuss results from Ref. [15] relevant to a centrosymmetric DAD molecule constituted by a central tetrafluorobenzene ring, phenylene vinylene as conjugated spacers, and terminal amino groups. For this chromophore a strong solvatochromism is observed in fluorescence, whereas the absorption band does not show any appreciable solvatochromism. Molecular model parameters can be readily estimated from spectroscopic data in non-polar solvent. The frequencies of the maximum of the linear absorption and TPA (ω_{ga} and ω_{ge}, respectively) fix ρ and $\sqrt{2}t$ [and hence η, see Eqs. (4), (5)]. The molecular parameters describing vibrational coupling, ω_v, ε_v, are fixed as to reproduce the Franck–Condon progression in absorption or fluorescence spectra. Finally, a band-width (HWHM) is associated to each transition as easily estimated from experimental spectra, and μ_0 is fixed to correctly reproduce the measured extinction coefficient. Relevant spectra are reported in the top panel of Fig. 3, and the TPA spectrum in a non-polar solvent is shown in Fig. 4, together with the OPA spectrum. Calculated spectra are in good agreement with experimental spectra in Ref. [15]: not only transition energies, and hence fluorescence solvatochromism, are well reproduced, but also band-shapes and absolute intensities of both OPA and TPA spectra compare favorably with experimental data.

Data on chromophores belonging to class **II** are scanty. Preliminary investigation suggests that some squaraine-based dyes may belong to this class of molecules. Indeed no major solvatochromic effects are reported for squaraines either in absorption or in fluorescence [12,24–27]. Large TPA cross sections are expected for dyes with intermediate quadrupolar character, but care has to be taken, since as $\rho \to 0.5$ we expect TPA absorption occurring just at twice the energy of the OPA: one-color TPA spectra would then be masked by large OPA signal.

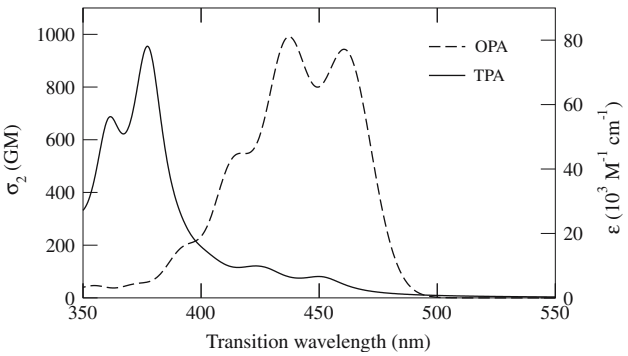

Fig. 4 One- and two-photon absorption spectra calculated for chromophore **1** in the apolar solvent

Symmetry-breaking (localization) in the excited state has been extensively investigated in recent years [2,28–34]. Specifically, the excited-state symmetry-breaking predicted by our model for chromophores of class **I** is in line with recent results in Ref. [2], where TD-DFT calculations predict the appearance of symmetry-broken solutions for the relaxed excited state of quadrupolar and octupolar chromophores. Our work generalizes these results for quadrupolar dyes, to account for solvation effects and their consequences in linear and nonlinear spectra. Even more importantly, the essential state model adopted here to describe the basic physics of quadrupolar chromophores leads to a general phase-diagram for this class of molecules.

3 Intramolecular ET and electrostatic interactions: clusters of push-pull chromophores

Results in the previous section demonstrate that environmental effects can be very important in systems with low energy ET degrees of freedom. Specifically, we have demonstrated that the unspecific interaction of a non-polar chromophore with a polar solvent, modeled as a continuum dielectric medium, can induce symmetry breaking in the ground or in the excited state. Even more important environmental effects are expected in dense systems where each chromophore, with its ET degrees of freedom, interacts with similar surrounding molecules. Here, as an example, we discuss linear arrays of DA chromophores, an interesting class of polar and polarizable molecules.

The electronic structure of push-pull chromophores is conveniently described by the Mulliken model [6,7], introducing two orthogonal basis states, $|N\rangle$ and $|Z\rangle$, corresponding to the neutral (DA) and zwitterionic (D^+A^-) resonance structures. The two states are separated by an energy 2η and mixed by a matrix element

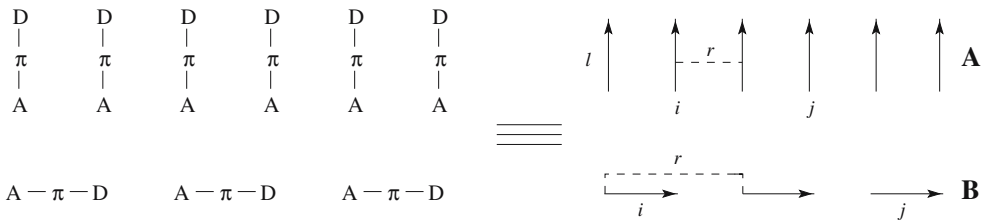

Fig. 5 The two one-dimensional arrays of chromophores discussed in this paper

$-\sqrt{2}t$. The diagonalization of the relevant Hamiltonian is trivial and was discussed by several authors [7]. The resulting ground and excited states are:

$$|g\rangle = \sqrt{1-\rho}\,|N\rangle + \sqrt{\rho}\,|Z\rangle$$
$$|e\rangle = \sqrt{\rho}\,|N\rangle - \sqrt{1-\rho}\,|Z\rangle \tag{9}$$

where the ionicity $\rho = (1 - \eta/\sqrt{\eta^2 + 2t^2})/2$ measures the weight of $|D^+A^-\rangle$ in the ground state (gs), and is therefore a measure of the molecular polarity. Following Mulliken [6,7], we recognize that in the adopted basis the dipole moment operator is dominated by μ_0, the dipole moment relevant to $|Z\rangle$, and, neglecting all other contributions, we obtain all spectroscopically relevant quantities as follows:

$$\mu_G = \langle g|\,\hat{\mu}\,|g\rangle = \mu_0\rho$$
$$\mu_E = \langle e|\,\hat{\mu}\,|e\rangle = \mu_0(1-\rho)$$
$$\mu_{CT} = \langle g|\,\hat{\mu}\,|e\rangle = \mu_0\sqrt{\rho(1-\rho)} \tag{10}$$
$$\hbar\omega_{CT} = \varepsilon_E - \varepsilon_G = \frac{\sqrt{2}t}{\sqrt{\rho(1-\rho)}}$$

On this basis, closed expressions for static NLO responses were written, that proved particularly useful since they relate linear and non-linear optical susceptibilities to spectroscopic observables [8]. Optical spectra of push–pull chromophores in solution can be described based on the same model, provided that it is extended to account for the coupling of electrons to slow degrees of freedom, including molecular vibrations and orientational degrees of freedom of polar solvents [10,11,35]. Both couplings are important in the definition of optical and static responses. Here we describe a model for clusters of interacting DA chromophores without accounting for slow degrees of freedom. As a matter of fact, in the adiabatic limit, vibrational coupling can be easily accounted for via a renormalization of the model parameters [36]. More generally, the non-adiabatic calculations needed to account for vibrational coupling in molecular clusters are memory and time-consuming, and so far have only been carried out on dimers of push–pull chromophores [37,38].

The Hamiltonian for a cluster of push-pull chromophores only interacting through electrostatic forces is [39]:

$$H = \sum_i \left[2\eta\hat{\rho}_i - \sqrt{2}t\,(|N_i\rangle\langle Z_i| + |Z_i\rangle\langle N_i|)\right] + \sum_{i,j>i} V_{ij}\rho_i\rho_j \tag{11}$$

where i and j run on the N molecular sites, and $\hat{\rho}_i = |Z_i\rangle\langle Z_i|$ measures the amount of CT from D to A in the ith molecules. The first term above corresponds to the two-state Mulliken model for the isolated chromophore, and the last term describes electrostatic interchromophore interactions. Since the expectation value of $\hat{\rho}_i$ fully defines the charge distribution on the ith chromophore, the operator representing the electrostatic interaction between i and j chromophores is proportional to $\hat{\rho}_i\hat{\rho}_j$ through a proportionality constant, V_{ij}, measuring the interaction energy between the two fully zwitterionic (D^+A^-) molecules. Of course several models are possible for V_{ij}, including dipolar or multipolar approximations, possibly accounting for electrostatic screening. The Hamiltonian above is general, here we apply it to describe two one-dimensional (1D) arrays of molecules as sketched in Fig. 5. Moreover, to estimate V_{ij}, we describe the zwitterionic molecule as a rigid rod of length l with the positive and negative charges located at the two ends. This defines the basic unit of electrostatic energy: $v = e^2/l$. In the following we discuss unscreened interactions and introduce the dimensionless inverse intermolecular distance, $w = l/r$, where r is the distance between the chromophores. For B-clusters the condition $w < 1$ applies. For any cluster V_{ij} interactions can be defined in terms of v and w parameters [39].

Intermolecular electrostatic interactions affect the molecular polarity. A molecule inside a cluster feels the electric field generated by the surrounding molecules. In clusters with repulsive interchromphore interactions (A in Fig. 5) each molecule feels an environmental electric field that opposes to the charge separation on each molecule, and the average polarity ρ on the molecular sites decreases. Just the opposite occurs for lattices with attractive interactions (B in Fig. 5), where one expects

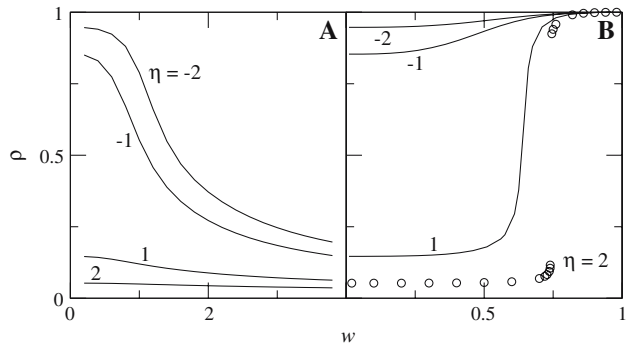

Fig. 6 The polarity of chromophores calculated as a function of w for two 1D arrays of 16 chromophores with $\nu = 2$ and the η marked in the figure. *Left panel*: repulsive interactions (A geometry); *right panel*: attractive interactions (B geometry)

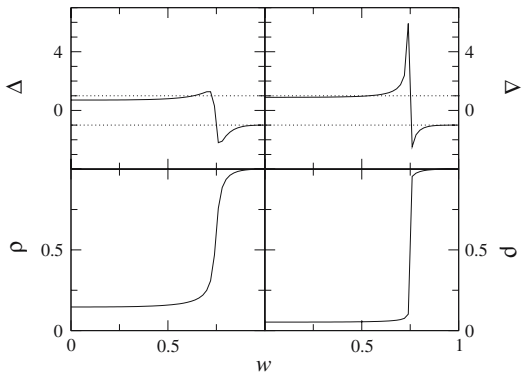

Fig. 7 *Upper panels*: number of zwitterionic species created upon photoexcitation (Δ) vs w. *Dotted lines* mark the boundary of the $|\Delta| < 1$ region allowed according to the exciton model. *Lower panels*: $\rho(w)$ curves for the same parameters as for the upper panels. Results are obtained for a 16-site B cluster. *Left panels*: $\nu = 1, \eta = 1$; right panels: $\nu = 2, \eta = 2$.

an increase of ρ with intermolecular interactions. This mean-field (mf) description catches most of the gs physics of molecular aggregates, and, specifically, allows one to appreciate the cooperative self-consistent interaction between each molecule and its environment [39].

Figure 6 shows the variation of the molecular polarity with the inverse intermolecular distance (w) for A and B clusters with different η. For the repulsive A lattice the most interesting results are obtained for negative η for which the isolated molecules at $w = 0$ are in a (zwitter)ionic (I) gs, with $\rho > 0.5$. In that case in fact simply putting the molecules together at a short enough distance turns all the molecule to a neutral (N) gs with $\rho < 0.5$.

N and I chromophores have qualitatively different properties and behavior, so intermolecular interactions can profoundly alter the material properties. Of course, for the attractive B-lattice the opposite occurs, and the most interesting case is that of chromophores with positive η. In that case in fact the N isolated molecule can turn to I in the lattice. Attractive lattices are even more interesting since for large enough ν the transition from a N to an I gs becomes discontinuous for suitable η values, as shown in the B-panel of Fig. 6 for $\eta = 2$. The observation of a discontinuous crossover is the extreme manifestation of cooperative behavior: two large competing interactions, η favoring the N gs, and the intermolecular interactions, favoring the I gs, lead to competing ground states whose energies cross at some special point in the parameter space giving rise to a discontinuous behavior.

The properties of the material in the proximity of the discontinuous N–I crossover are very interesting and unusual [40]. Focusing on the optical excitation with the largest oscillator strength (that always coincides with the lowest excitation, E_1 in B-lattices) we calculate the number of $|Z\rangle$ molecules that are created upon photoexcitation, or, equivalently, the number of electrons that are transferred from D to A: $\Delta = N\big(\langle E_1|\,\hat{\rho}\,|E_1\rangle - \langle G|\,\hat{\rho}\,|G\rangle\big)$ (negative Δ means that electrons are transferred from A^- to D^+). In the familiar excitonic approximation [41] the absorption of a photon creates a single excitation, switching a molecule from the local ground to the local excited state: in this approximation $\Delta = 1 - 2\rho$ and the number of transferred electrons upon photoexcitation ranges from 1 for largely N lattices ($\rho \to 0$) to -1 for largely I lattices ($\rho \to 1$). The upper panels in Fig. 7 show the evolution with w of Δ, calculated for a 16-site B lattices with a continuous and a discontinuous neutral to zwitterionic interface (left and right panels, respectively, cf. bottom panels, where the relevant $\rho(w)$ curves are shown). The dotted lines mark the extreme limits of the excitonic approximation for Δ, i.e. $|\Delta| < 1$. The simple excitonic result is spoiled near the charge crossover: deviations are minor near a continuous interface (left panels), but become important near a discontinuous interface: for the parameters in Fig. 7, up to six electrons are transferred at a time upon absorption of a single photon.

A detailed analysis of the states involved in absorption leads to a very interesting picture [40]. Upon absorption of a single photon in fact several I chromophores are created on a background of N molecules or vice versa, and these molecules with *reversed* ionicity cluster together forming a droplet of I (N) molecules on a N (I) background. Multi-electron transfer has already been discussed in different contexts, but usually describes a cascading effect related to the relaxation of some slow degree of freedom following a more traditional optical excitation [42,43]. Here instead multi-electron transfer represents the *primary photoexcitation event*: the absorption of a single photon directly drives the

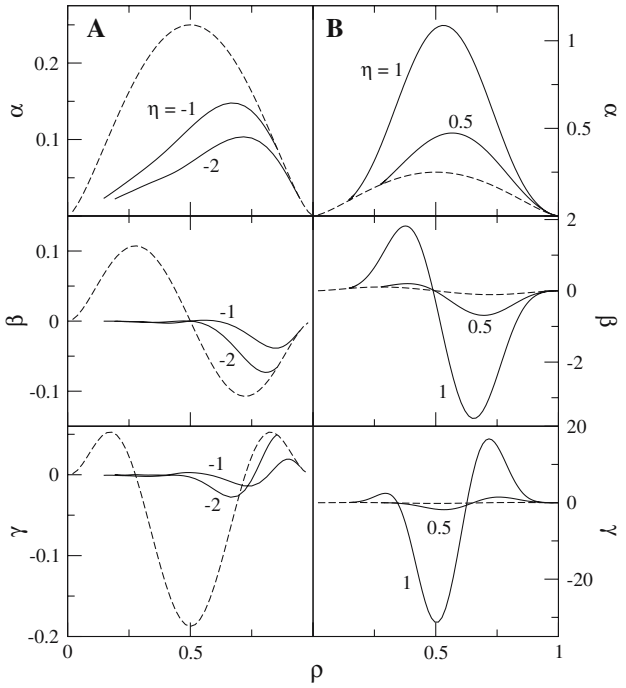

Fig. 8 Static polarizability and hyperpolarizabilities per chromophore calculated for clusters of 16 push–pull chromophores with repulsive (**a**) and attractive (**b**) interactions and $v = e^2/l = 2$. Results are shown for the selected η marked in the figure and are obtained by varying w as to obtain the ρ values reported in the x-axis. In all panels dashed lines show the (hyper)polarizabilities relevant to the isolated push–pull chromophore: these curves are of course equal in the *left* and *right panels*, their different appearance is due to the largely different scales needed to show in the same panel results for the isolated molecule and for the cluster.

concerted motion of several electrons residing in several nearby molecules.

Important effects from supramolecular interactions are also expected in NLO responses [30]. Figure 6 shows very clearly that the polarity of a chromophore is strongly dependent on its environment, and, specifically, on the geometry of the cluster, and on intermolecular distances. It is known that linear and non-linear polarizabilities of isolated push–pull chromophores are fixed by ρ [8]. So, when considering clusters of push-pull chromophores one expects that their susceptibilities vary with the cluster geometry and intermolecular distance, due to the variation of ρ. Indeed the situation is much more complex, with important cooperative and collective contributions to the cluster susceptibility. This is clearly demonstrated by data in Fig. 8 where the linear polarizability α and the first and second hyper-polarizabilities, β and γ, respectively, are shown as a function of ρ. Results are obtained for A (repulsive interactions) and B (attractive interactions) with $v = e^2/l = 2$ and selected η values, while varying w as to span a large interval of ρ (cf. Fig. 6). The dashed lines in the same figure show the linear and non-linear susceptibilities of the isolated chromophore, that only depend on ρ [8]. The deviations of the cluster susceptibilities from the result relevant to the isolated chromophore with the same polarity measure cooperative and collective effects that derive from local-field corrections, as well as from the excitonic and ultraexcitonic mixing of excited states. The role of the different interactions has been recently discussed [3], here we underline that cooperative and collective contributions to the susceptibilities are very large and rapidly increase with the order of non-linearity. In A geometry the cluster response is largely suppressed with respect to the molecular response, whereas in B geometry a very large amplification is observed. A well known result for the isolated chromophore is the symmetry of the responses around $\rho = 0.5$, the so-called cyanine limit. This result is spoiled by electrostatic interactions in the cluster.

Materials based on push–pull chromophores have negligible intermolecular overlap, and we have discussed here a model where electrons are fully localized in the molecular units. In spite of that, electrostatic intermolecular interactions make ET in clusters qualitatively different from ET in the isolated chromophore. In the quest for materials with optimized properties it is then extremely important to properly understand and exploit *supramolecular* structure–function relationships. This is a challenging task, due to the need to account for complex cooperative and collective phenomena, but it may also be a largely rewarding job as it offers an additional handle to tune, and possibly amplify, the material response.

4 Extended systems and electrostatic interactions: charge-transfer salts with a mixed stack motif

Charge-transfer (CT) crystals have mixed face-to-face stacks of planar π-electron donors and acceptors as sketched in Fig. 9. Intermolecular overlap is negligible between stacks, but not within stacks where π–π overlap is indicated by less than van der Waals separation between D and A [45]. The gs consequently has fractional charges ρ at D and $-\rho$ at A sites [45]. Just as an example, in the prototypical material, TTF-CA, at ambient conditions about 0.2 electrons are transferred on average from the donor (tetrathiafulvalene, TTF) to the acceptor (chloranil, CA) [4]. We notice that while referring to different physical systems with respect to those described in the previous section, the parameter ρ corresponds to the same physical quantity. Specifically in both systems ρ measures the fractional charge on D/A sites: in push-pull chromophores the sites correspond to

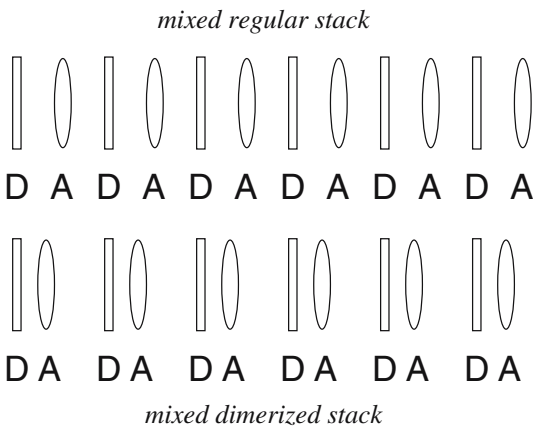

Fig. 9 A schematic view of mixed regular and dimerized stacks

different chemical groups in the same molecule, in CT salts to different molecular units. In both cases the fractional ionicity is a direct consequence of ET.

As seen in Fig. 9, a regular stack of centrosymmetric molecules is not polar due to the inversion center located at each site, as in fact occurs in the actual structures. The inversion center is lost on dimerization and the gs becomes ferroelectric if dimerization is in the same sense everywhere. Much as it occurs in attractive lattices in the previous section, Madelung interactions favor charge separation, and a large variation of ρ can be induced by tuning intermolecular distances. At $T \sim 81$ K, TTF-CA undergoes a discontinuous phase transition to an I phase with $\rho \sim 0.6$ [4]. Other systems with N–I transitions are known [4]: both continuous and discontinuous transitions have been observed, and stack dimerization typically accompanies the charge crossover. In a CT crystal with disordered site energies, due to orientational disorder of the polar D, however, the ionic stack does not dimerize [46] . N–I transitions can be induced by temperature, pressure or by absorption of light and represent a complex and interesting phenomenon [47,48].

Mixed stack CT salts share some physics with B-lattices of push–pull chromophores discussed in the previous section. Indeed one of the first models for the discontinuous N–I transition in CT salts [49] was based on the description of the stack as a collection of DA pairs only interacting via electrostatic interactions leading exactly to the same Hamiltonian as discussed in the previous section. More realistic models for the stack must account for delocalized electrons in 1D [50]. Moreover, in order to properly describe structural instabilities, models for CT salts must also include the coupling between electrons and lattice phonons [51,52]. A minimal model for the gs of CT salts with a mixed stack motif is represented by the following Hamiltonian [51,52]:

$$H = -\sum_{i,\sigma}\left[1+(-1)^i\delta\right]\left(c^+_{i,\sigma}c_{i+1,\sigma} + H.c.\right) + \Gamma\sum_{i,\sigma}(-1)^i c^+_{i,\sigma}c_{i,\sigma} + V\sum_i \rho_i\rho_{i+1} + \frac{N}{2\varepsilon_d}\delta^2 \qquad (12)$$

where $c^+_{i,\sigma}$ creates an electron with spin σ on the ith site and the number operator, $\hat{n}_{i,\sigma} = c^+_{i,\sigma}c_{i,\sigma}$ is restricted to 0 or 1 on A sites (i even) and to 1 or 2 on D sites (i odd). The first term is the Hückel model for electron transfer between neighbors in the stack; we take $t = -\langle DA|H|D^+A^-\rangle = 1$ as the energy unit, and $t_i = [1-\delta(-1)^i]$ for dimerized stacks. The second term has site energies $-\Gamma$ at D and $+\Gamma$ at A. The third term is the nearest neighbor Coulomb attraction V that in mean field (mf) adds $-V\rho$ to Γ; the charge operator ρ_i is $2-n_i$ at D sites and $-n_i$ at A sites. Since the full electrostatic (Madelung) energy of the crystal leads to similar modification of Γ in mf theory, at this level V represents any Coulomb or vibronic interaction that modifies sites energies. The last term in the above Hamiltonian measures the bare elastic energy associated with the dimerization mode, with $1/\varepsilon_d$ measuring the lattice stiffness. The rigid lattice has $\varepsilon_d = 0$.

For $\Gamma >> V$ the Hamiltonian in Eq. (12) describes an almost N lattice ($\rho \to 0$) of donors and acceptors, whereas for $\Gamma << V$ an almost I lattice of spin 1/2 radical ions is obtained ($\rho \to 1$) [50]. The N–I crossover is continuous for small V, but becomes discontinuous at large V [53]. The N and I phases are qualitatively different, with the I lattice being unconditionally unstable to dimerization (spin-Peierls transition [55]). The N–I crossover can consequently be identified precisely even for continuous ρ in the rigid regular stack [53,54]. The possible occurrence of two instabilities leads to a complex phase diagram: soft lattices dimerize in the N phase before reaching the N–I crossover. Harder lattices with sizeable V instead undergo a discontinuous transition from a N regular to an I dimerized phase. Both kinds of transitions have been observed [4].

Figure 10 summarizes results obtained on a system with large enough V and small enough ε_d as to undergo to a discontinuous charge crossover, as evidenced by the $\rho(\Gamma)$ curve in the rightmost panel. The middle panel in the same figure shows the dimerization amplitude: the stack is regular in the N regime and dimerizes in the I phase mimicking TTF-CA. The discontinuous N–I crossover in Fig. 10 closely resembles the discontinuous crossover described in the previous section for the linear cluster of push–pull chromophores, and, as already noticed, the two systems indeed share some physics. However the physics of the N–I transition in CT salts is much more complex than in push–pull chromophores since electrons are now truly delocalized in 1D, and a

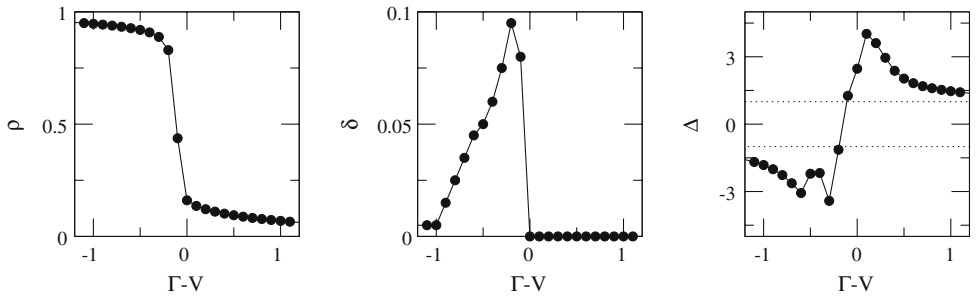

Fig. 10 The N–I transition for a CT salt described by the Hamiltonian in Eq. (12) with $V = 3$, and $\varepsilon_d = 0.28$. Results are shown for a 12 site chain. *Left* and *middle panels* show the evolution with Γ of the ionicity and of the dimerization amplitude, respectively. The *right panel* shows the number of D^+A^- pairs created upon photoexcitation (results refer to the optical transition with the highest intensity). The two *dotted lines* in this panel at $\Delta = \pm 1$ mark the limits for Δ in the excitonic approximation

lattice instability accompanies the charge instability. In spite of that, the intriguing phenomenon of multi-electron transfer survives in CT salts, as shown in the rightmost panel of Fig. 10, where the number of D^+A^- pairs created on photoexcitation is reported. For the parameters in Fig. 10, that apply to TTF-CA [52], we find that at the N–I interface the absorption of a single photon moves as many as four electrons at a time. The analysis of the relevant wavefunction demonstrates that, much as it occurs for clusters of push–pull chromophores, photoexcitation generates droplets of I states in an otherwise N background (or vice versa). These droplets, created upon vertical phoexcitation, can act as nucleation centers for the photoinduced NIT and can explain the high quantum yield of the process close to the thermally-induced transition [43].

Not only optical spectra, but also gs properties, including linear and non-linear polarizabilities show unusual behavior at the charge crossover. Here we discuss the linear polarizability, that, being related to the static dielectric constant, has important experimental implications. The static polarizability is the first derivative of the polarization on the applied electric field, $\alpha = \mathrm{d}P/\mathrm{d}F$, and can be calculated in finite-field approaches from the $P(F)$ dependence, or, in sum-over states approaches as the sum over all excited states of the squared transition dipole moments over the relevant excitation frequencies [56].

The calculation of $P(F)$ and hence of α is straightforward in principle in systems with localized electrons, like the clusters of push–pull chromophores described in the previous section. In that case in fact the linear chain can be naturally partitioned in non-overlapping unit cells. The dipole moment operator $\hat{M}$ is then defined as the sum of dipole moments on each cell and enters the F dependent Hamiltonian as $-F\hat{M}$, allowing the calculation of F-dependent properties. Numerical F-derivatives of P or its perturbative expansion in sum over state approaches are both viable and lead to equivalent results for α. The situation is more complex in extended systems where delocalized electrons make the partitioning of the system in unit cells non-unique. The Berry-phase definition of P for extended systems, or, equivalently for finite systems with periodic boundary conditions (PBC), solves the problem of the calculation of $P(F = 0)$ [57], but leaves open the calculation of F-dependent properties.

In fact, the lack of an explicit definition for the electric dipole moment operator in PBC systems, hinders both the definition of the F-dependent Hamiltonian $H(F)$ and the calculation of transition dipole moments entering sum over states expressions for the susceptibilities. We have recently solved this problem by introducing an induced dipole operator [52]:

$$\Delta\hat{M} = \frac{N}{2\pi}\,\mathrm{Im}\,\frac{\exp(2\pi i\hat{M}/N)}{Z(F)} \tag{13}$$

where $\hat{M} = \sum_i r_i\rho_i$ is the traditional dipole moment defined for the open chain and $N/2$ is the number of unit cells, and

$$Z(F) = \left\langle G(F)\left|\exp\left(\frac{2\pi i\hat{M}}{N}\right)\right|G(F)\right\rangle \tag{14}$$

where $|G(F)\rangle$ is the gs of $H(F)$. $\Delta\hat{M}$ enters the definition of an effective Hamiltonian $H(F) = H - F\Delta\hat{M}$, whose diagonalization is equivalent to the minimization of the energy functional $E(F, G(F)) = \langle G(F)|\,H\,|G(F)\rangle - NF\,\mathrm{Im}(\ln(Z(F))/2\pi$, where H is the unperturbed Hamiltonian. The procedure is formally exact when working on a real space basis where $\hat{M}$ is diagonal. Moreover, except for the linear polarizability, which requires Z (0) in Eq. (13), $|G(F)\rangle$ must be found iteratively [52].

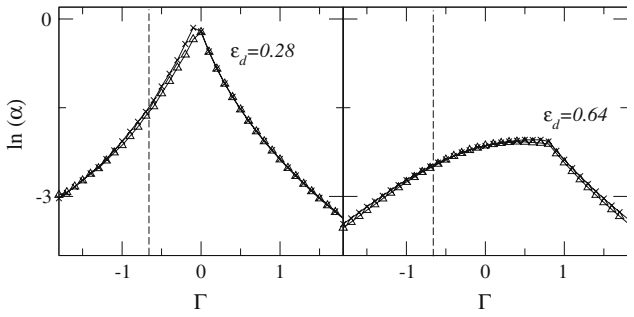

Fig. 11 The logarithm of the linear electronic polarizability vs Γ for a mixed stack with $V = 0$ and for the ε_d values in the figure. Triangle and crosses refer to $N = 12$ and 14, respectively. The dashed line marks in each panel the location of the N–I transition in the rigid ($\varepsilon_d = 0$) chain

Along these lines we have demonstrated that the linear polarizability calculated for the rigid chain diverges at the continuous NIT of the regular chain with $V = 0$. The dashed line in Fig. 11 locates the electronic transition of the rigid lattice, where the gs is metallic [50]. The divergence is however suppressed by dimerization in soft lattices with $\varepsilon_d > 0$ as shown in Fig. 11, where the kink in α marks the Peierls transition.

So far we have discussed the linear electronic polarizability calculated as the first derivative of P on the electric field while keeping the nuclei at their equilibrium location. This electronic polarizability does not exhaust the material polarizability. In fact due to the coupling between electronic and lattice degrees of freedom we expect a vibrational contribution to α, with [36,37]:

$$\alpha = \frac{\partial P}{\partial F} + \frac{\partial P}{\partial \delta}\frac{\partial \delta}{\partial F} = \alpha_{\rm el} + \alpha_{\rm vib} \tag{15}$$

The vibrational contribution to the polarizability is governed by the lattice vibration corresponding to the dimerization motion, as described by δ. Specifically $\alpha_{\rm vib}$ goes with the IR intensity of the dimerization mode divided by its frequency. Close to the charge-instability, δ oscillations induce large fluxes of electronic charge from D to A sites and vice versa leading to gigantic IR intensity of the Peierls mode near the N–I interface [36]. Moreover, the Peierls mode drives the dimerization instability, and its frequency softens in the proximity of the lattice instability. As a consequence, the vibrational contribution to the polarizability is very large and actually dominates over the electronic contribution for systems close to the charge and structural instability [51,52].

Both $\alpha_{\rm el}$ and $\alpha_{\rm vib}$ contribute to the static dielectric constant, according to

$$\kappa = \kappa_\infty + \frac{\alpha_{\rm el} + \alpha_{\rm vib}}{\varepsilon_0 v_0} \tag{16}$$

where SI units are adopted, v_0 is the volume per site, ε_0 is the vacuum permittivity constant, and $\kappa_\infty \approx 3$ is the usual contribution to the dielectric constant from molecular excited states that are not being modeled. Adopting typical lattice parameters for TTF-CA we obtain the κ values reported in a logarithmic scale in the left panels of Fig. 12. A sharp peak in κ is observed with absolute values of the order of 100–1,000, in agreement with experimental data [47,48]. Specifically, the figure shows results obtained for $V = 0$ and two different ε_d values. The harder lattice in the left panels dimerizes at $\rho \sim 0.4$, in the near proximity of the charge instability: the coupling between electronic and vibrational degrees of freedom is very large here and the resulting κ is very large. The softer lattice dimerizes far in the neutral regime, at $\rho \sim 0.25$, where charge fluctuations induced by δ are smaller: the calculated peak in the dielectric constant is reduced by almost one order of magnitude with respect to the previous case. In both cases however, κ is dominated by the vibrational contribution: the result obtained by neglecting $\alpha_{\rm vib}$ in Eq. (16) is shown as dotted lines in Fig. 12 and represents a negligible fraction of the dielectric constant. Results for systems with finite and large V as to describe discontinuous N–I transitions have already been discussed [52] . Here we just notice that $V = 0$ results are enough to describe the behavior of a system with finite V in the mf approximation. Within mf in fact V enters the Hamiltonian via a renormalization of $\Gamma \to \Gamma - V\rho$. For $V > (\mathrm{d}\rho/\mathrm{d}\Gamma)^{-1}/2 \approx 2.5$ the N–I transition becomes discontinuous and regions of intermediate ρ are no more accessible to the system. This leads to a reduction of the κ peak that, for $\varepsilon_d = 0.28$ reduces from ~ 1000 at $V = 0$ to ~ 150 at $V = 3$.

5 Electron transport in molecular junctions: a real-space view

ET is the basic process for electron transport in molecular junctions. In spectroscopic measurements ET implies the hop of one (or more) electron from a D to an A site, to create an excited state that eventually relaxes back to equilibrium. In molecular electronic devices instead a continuous flux of charges must be maintained: to sustain a direct current (DC) the system must be prepared in a non-equilibrium steady-state. The most popular approaches to describe molecular junctions are based on the Bütticker–Landauer picture [58,59]: the junction, i.e. the molecule possibly including atoms from the contact region, is embedded between two semi-infinite electrodes working as source and sink for the electrons. The electrical flux is driven by imposing a finite potential

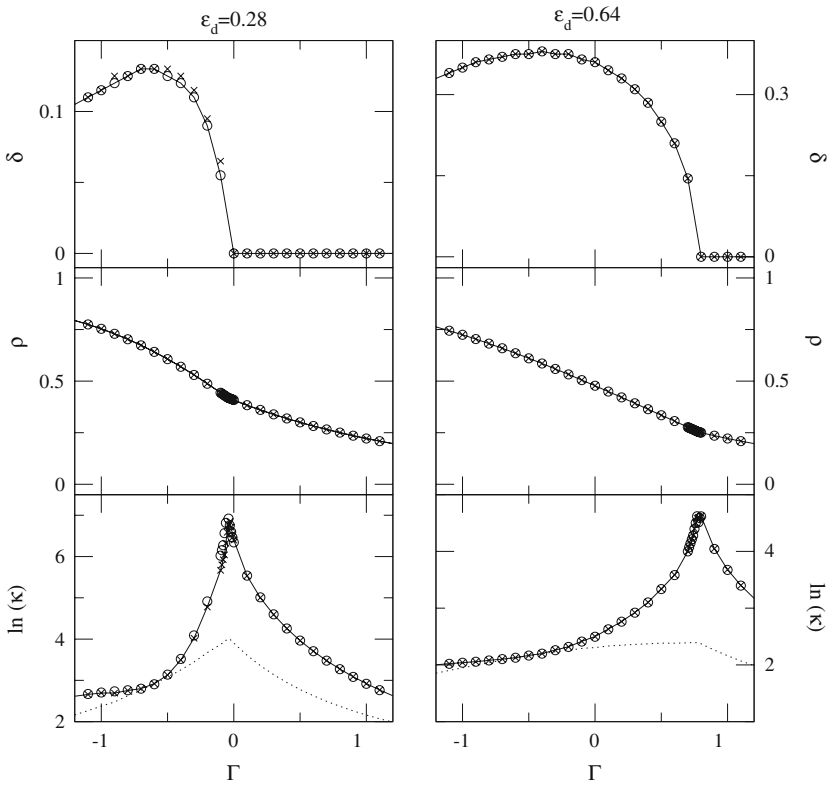

Fig. 12 The dimerization amplitude, the ionicity and the logarithm of the static dielectric constant, as a function of Γ calculated for the Hamiltonian in Eq. (12) with $V = 0$ and two different ε_d. Circles refer to $N = 14$, crosses to $N = 16$. Dotted lines in the bottom panels show the logarithm of the dielectric constant obtained by neglecting the vibrational contribution to α

drop between the two electrodes to enforce a net flux of charges from the high to the low potential region.

This voltage constrained (VC) approach proved very successful to describe mesoscopic and nanoscopic junctions and has been quite naturally combined with detailed first-principles models for the molecular structure and the contact region [5,60]. However, working with infinite reservoirs poses some fundamental physical problems [61–65], among which the need to account, in the same quantum mechanical system, for two families of electrons with different chemical potential, and, henceforth, the need to rely on one-electron models for the electronic structure.

Any reference to reservoirs is avoided in current constrained (CC) approaches, that have been developed to describe transport in both meso- and molecular junctions [61,62,66–69]. Closed boundary conditions are imposed on the system, and a current is forced through the circuit, via some physical or mathematical device. CC and VC approaches are therefore complementary and, in a sense, describe two different experiments, where either the current or the potential drop is fixed from the outset [69]. The Lagrange multipliers technique represents an interesting mathematical device to drive a molecule in a non-equilibrium state as to force a current through it. This technique has a long history in the field of mesoscopic transport [69] and has been more recently adopted to describe molecular junctions [62,68].

Whereas CC strategies are promising, two main problems remain to be solved: (1) the calculation of the potential drop needed to sustain the current, and (2) the definition of the potential profile in the molecule. To solve the first problem we take advantage from energy conservation as described by the Joule law: in a system with fixed current, the potential drop can be obtained from the electrical work done on the junction to sustain the current. Charge-conservation is the key to solve the second problem: enforcing the continuity constraint for DC transport leads to the definition of the potential profile along the junction. The approach is general: here we sketch its application to linear Hubbard chains.

To start with consider a diatomic Hubbard molecule, whose Hamiltonian H_0 is defined by U, t, and the difference of on-site energies: $2\Delta = \varepsilon_2 - \varepsilon_1$. The eigenstates of H_0 do not sustain any current. To impose a finite steady-state current the molecule is prepared in a non-equilibrium state $|G(\lambda)\rangle$, defined as the ground state of the Hamiltonian [68]:

$$H(\lambda) = H_0 - \lambda \hat{j} \tag{17}$$

where $\hat{j} = -it \sum_\sigma \left(c^+_{1\sigma} c_{2\sigma} - H.c.\right)$ measures the current flowing through the bond, and $c_{i\sigma}$ annihilates an electron with spin σ on the i-site. Here and in the following $\hbar$ and the electronic charge are set to 1, and t is taken as the energy unit. The field λ coupled to the current enters

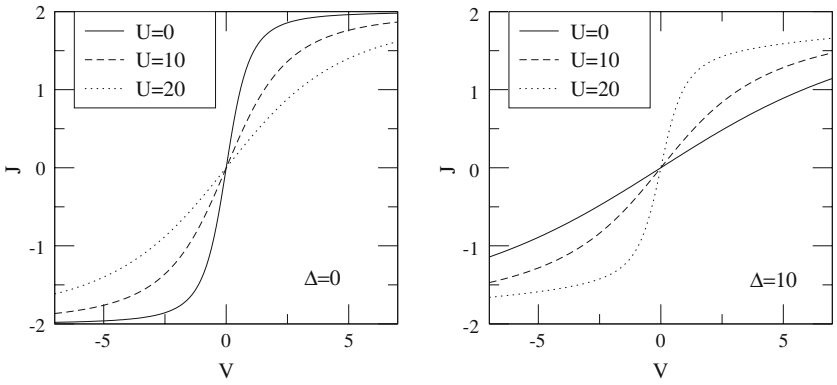

Fig. 13 Characteristic $J(V)$ curves for a two-site system. Depopulation and dephasing rates are set as to impose $\Gamma_{km} = 1$

the Hamiltonian above as a Lagrange multiplier, whose value is fixed by the requirement that a finite current $J = \langle G(\lambda)|\hat{j}|G(\lambda)\rangle$ flows through the molecule [68].

In the absence of relaxation $|G(\lambda)\rangle$ would be a stable state and the current will flow with no resistance. Relaxation instead drives the molecule towards the unperturbed equilibrium state $G(0)$ so that work must be spent to maintain the molecule in the current-carrying state. Of course, to grant for steady state conditions, the device must dissipate exactly the same amount of energy. The Joule law defines the relation between the electrical power spent on the molecule, W, and the potential drop needed to sustain the current, $W = JV$, underlining the fundamental relation between resistance and relaxation [64].

Following standard approaches in molecular spectroscopy relaxation is described introducing the density matrix written on the basis of the eigenstates $|k\rangle$ of $H(0)$ [1]. The equilibrium density matrix for the molecule in the absence of the driving field, σ_0, is a diagonal matrix whose elements are fixed by the Boltzmann distribution. Here we work in the low temperature limit, so that only the lowest eigenstate, $|G(0)\rangle = |g\rangle$ is populated. In non-degenerate systems, the current operator is off-diagonal, so that $\sigma(\lambda)$, the density matrix for the current-carrying state, is non-diagonal: finite *coherences* (i.e. off-diagonal elements of the density matrix) are needed to describe a current. The dynamical equation for σ is: $\dot{\sigma} = -\mathrm{i}[H, \sigma] + \dot{\sigma}_R$, where $\dot{\sigma}_R$ accounts for relaxation phenomena, as due to the coupling of the molecule to the bath, i.e. to all degrees of freedom not explicitly described by H. Diagonal elements of $\dot{\sigma}_R$ describe depopulation, i.e. *inelastic scattering* events that dissipate energy to the bath. We adopt a phenomenological model for depopulation [1], and set $(\dot{\sigma}_R)_{kk} = \sum_m \gamma_{km}\sigma_{mm} - \sum_m \gamma_{mk}\sigma_{kk}$, where γ_{km} measures the probability of the transition from m to k. In the low-temperature limit, only downwards transitions occur: $\gamma_{km} = 0$ for $k > m$. Γ_{km}, the inverse lifetime for coherences, is defined by $(\dot{\sigma}_R)_{km} = -\Gamma_{km}\sigma_{km}$, and has both depopulation and dephasing contributions: $\Gamma_{km} = (\gamma_{kk} + \gamma_{mm})/2 + \gamma'_{km}$, where $\gamma_{kk} = \sum_{m\neq k}\gamma_{mk}$ is the inverse lifetime of state k as due to depopulation, whereas γ'_{km} describes pure dephasing, i.e. the loss of coherence due to purely *elastic scattering* [1].

Relaxation dynamics is affected by the electrical contacts. This is easily understood in single electron pictures: electrons are strongly scattered at the junctions and neither the elastic nor the inelastic lifetime can be longer than the time required to the electron to cross the junction [63]. For correlated electrons the effects of leads on relevant lifetimes are more subtle, and a microscopic model is still lacking. However, even in the limit of very weak coupling, when electrons hardly hop from the molecule to the leads, the very same presence of a metallic surface close to the molecule opens new energy exchange channels that decrease the inelastic lifetime. In the case of strong coupling, the blurring of the discrete molecular eigenstates as due to their mixing with the continuum of states of the metallic leads is responsible for large dephasing rates.

The electrical work, $W = -\lambda Tr\left(\dot{\sigma}_R\hat{j}\right)$ measures the electrical power spent on the molecule to sustain the current. Since $\hat{j}$ is an off-diagonal operator, only off-diagonal elements of σ'_R enter W. Therefore V and hence the molecular resistance are governed by the total lifetime for coherences, Γ_{km} quite irrespective of its partitioning into elastic and inelastic scattering (dephasing and depopulation, respectively) contributions [64].

Figure 13 shows the characteristic curves calculated for a diatomic molecule with $\Gamma_{km} = 1$. In the left panel results are shown for the symmetric, $\Delta = 0$, system. As expected, electronic correlations decrease the conductivity. The curves in the right panel for an asymmetric system ($\Delta \neq 0$) show instead an increase of the low-voltage conductivity with increasing U. This result is related to the minimum excitation gap, and hence the maximum conductance, of the system with $U = 2\Delta$. The asymmetric diatomic molecule represents a minimal

model for the Aviram-Ratner rectifier [70], but the characteristic curves in the right panel of Fig. 13 are symmetric, and do not support rectification. In agreement with recent results, rectification in asymmetric molecules is most probably due to contacts [60], or to the coupling between electrons and vibrational or conformational degrees of freedom [71].

An important result may be found for the symmetric two-site system with a single electron. Via a perturbative expansion of the current, a very simple expression for the zero bias conductivity is found: $\mathcal{G}_0 = t/\Gamma$. Since the electronic lifetime, Γ, cannot be longer than the time required to the electron to hop between the two sites [63], we can set $\Gamma \geq 2\pi t$, regaining the standard result for the conductivity of a single electron: $\mathcal{G}_0 = 2\pi$ (in units with $\hbar = e = 1$).

To extend the discussion to linear polyatomic chain an important point must be appreciated: DC transport requires charge conservation both at the global and at the local level. In other terms, during transport charge must not accumulate. To enforce the continuity constraint one must control the current flowing through every bond in such a way that in a linear chain exactly the same amount of current flows through each bond. To such an aim the following Hamiltonian is introduced:

$$H = H_0 - \sum_i \lambda_i \hat{j}_i \tag{18}$$

where i runs on the bonds and the Lagrange multipliers, λ_i, are fixed by imposing $j_i = \langle G|\hat{j}_i|G\rangle = J$, independent of i. The electrical work spent on the molecule:

$$W = -\sum_i \lambda_i Tr\left(\hat{j}_i \dot{\sigma}_R\right) \tag{19}$$

naturally separates into bond-contributions, W_i, and the total potential drop across the molecule, $V = W/J$, can be written as the sum of the potential drops across each bond, $V_i = W_i/J$, leading in general to non-linear potential profiles. The relevant information is conveniently conveyed in terms of bond-resistances: $R_i = (\partial J/\partial V_i)^{-1}$ [64].

Figure 14 shows the results obtained for a three-site three-electron molecule with $U = 4$, $\Gamma_{km} = 1$, equal on-site energies and different t. The left panel shows the characteristic $J(V)$ curve, and continuous lines in the right panel report the total resistance R, and the two bond resistances, R_1 and R_2. As a direct consequence of the continuity constraint, the total resistance $R = (\partial J/\partial V)^{-1}$ is the sum of the two bond-resistances, leading to a suggestive description of the linear molecule as an electrical circuit, with resistances associated with chemical bonds joint in series at the atomic sites. Whereas this picture is useful, the concept of

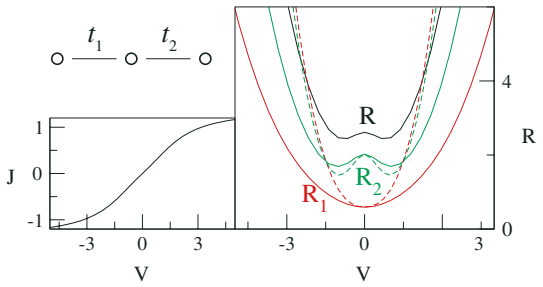

Fig. 14 *Left panel*: characteristic curve for the three-site three-electron Hubbard molecule sketched in the figure, with $U = 4$, constant on-site energies, $t_1 = 1.2$, $t_2 = 0.8$, $\Gamma_{km} = 1$. *Right panel*: total (R) and bond-resistances (R_1 and R_2). For bond resistances continuous and dashed lines show results obtained by allowing the current to flow through the whole molecule, and through a single bond, respectively

bond-resistance should be considered with care in molecular circuits. At variance with standard conductors, in fact, the resistance of a bond depends not only on the circuit (the molecule) it is inserted in, but also on the way the resistance is measured. In fact the resistance of each bond can also be defined by forcing the current only through the specific bond (i.e. by setting a single $\lambda_i \neq 0$ in the Hamiltonian in Eq. (18)). Dashed lines in Fig. 14 show corresponding results. At zero bias, for each bond the two kinds of resistance do coincide (as it can also be proved by perturbative arguments) so that the molecular resistance is the sum of the bond-resistances measured by flowing current through each bond. This *additive* Ohmic behavior is however spoiled at finite bias (cf. Fig. 14), or even at zero bias when allowing for more complex relaxation matrices with non-uniform Γ_{km}.

Multiple Lagrange multipliers account for non-linear potential profiles in polyatomic molecules: modeling the potential profile as a linear function is a poor approximation for extended molecules [72]. Just as an example, in a four-site four-electron junction with exactly the same $t_i = 1$ on each bond, the central bond is much weaker than the two external bonds leading to a ratio of the zero-bias resistances, R_2/R_1, ranging from 10 to 2 as U increases from 0 to 4. Largely non-linear potential profiles are therefore expected even for highly idealized molecular structures.

Current and voltage constrained approaches to molecular junctions offer complementary views of the same phenomenon and, having each one its merits and drawbacks, both should be carefully explored to reach a comprehensive representation of the complex physics of molecular transport. One of the most appealing features of CC approaches is the possibility to work with correlated electrons. Here we fully exploit this opportunity combining the CC description of transport with a real-space description of the molecule. The resulting picture

is strongly rooted in the concept of chemical bond: chemical bonds offer channels for electronic transport, i.e. the current flows through the bonds. This view should be contrasted with the more familiar picture of electrons flowing through molecular orbitals, as resulting from the typically one-electron description of molecular junctions adopted in VC approaches. Neither picture is more fundamental or more correct than the other: they correspond and actually stem from the two complementary and equally fundamental descriptions of molecular binding as based on the molecular orbital or valence bond descriptions [73]. Both are important and should be known to fully appreciate the complex realm of molecular physics.

6 Conclusions

In this paper we have described several classes of materials and systems where ET plays an important role. We have focused attention on the spectroscopic behavior of materials with low-energy charge-transfer excitations, and on electron transport in molecular junctions. As for spectroscopy we have underlined the main role of environmental interactions. Non-polar DAD chromophores, extensively studied for TPA applications, show a strongly solvatochromic fluorescence, whose origin we ascribe to the symmetry-breaking induced in the excited states by unspecific interactions with the polar solvents. The model is general and applies to other classes of molecules as well.

Collective and cooperative behavior appears as a consequence of the electrostatic interactions between ET processes occurring at different location in materials like clusters of DA chromophores and CT crystals. Important collective and cooperative phenomena show up clearly in static susceptibilities of clusters of push–pull chromophores. Classical electrostatic intermolecular interactions lead to a suppression of the optical susceptibilities in the repulsive A-lattice and to an amplification in the attractive B-lattice in Fig. 5, with effects that increase fast with the order of non-linearity.

In CT salts it is more difficult to single out the role of electrostatic interactions, due to the complex interplay among delocalization effects, electrostatic 3D interactions, and lattice phonons. The electronic contribution to the static linear polarizability in CT salts is enormously amplified by delocalization: in fact, even in the absence of electrostatic interactions, the polarizability diverges at the continuous NIT of the rigid lattice. However in soft lattices electron–phonon coupling drives the lattice dimerization, reducing the electronic delocalization and strongly suppressing the electronic contribution to the polarizability. At the same time, a vibrational contribution adds to the polarizability, becoming largely dominant over the electronic contribution in the proximity of the dimerization phase transition.

Both in systems with electrons localized within discrete molecular units and in materials with delocalized electrons in 1D, electrostatic interactions can lead to the occurrence of a discontinuous charge crossover, and hence to the appearance of bistable behavior. In the proximity of discontinuous crossovers cooperative and collective phenomena dominate and multielectron transfer represents the most striking demonstration of that. The possibility to induce a concerted motion of several electrons upon absorption of a single photon contrasts sharply with the common excitonic description of optical excitations in molecular materials and opens interesting and new perspectives for the understanding of photoinduced phase transitions and for applications in photoconversion devices.

A current constrained approach is proposed to describe electron-transport in real-space description of molecular junctions. Along these lines a picture emerges where electron transport occurs through chemical bonds. This picture is complementary to the more common picture emerging from voltage constrained approaches that describe electrons flowing through molecular orbitals. Molecular resistance is quite naturally ascribed to the relaxation of molecular states as due to both elastic and inelastic scattering (i.e. depopulation and dephasing). Relaxation is just the connection between the diverse fields of molecular transport and molecular spectroscopy: here we have described relaxation based on a phenomenological model borrowed from molecular spectroscopy. At the same time, specific features of molecular junctions must be recognized: the continuity constraint for steady-state DC current has no counterpart in molecular spectroscopy and is responsible for the appearance of non-linear potential profiles in extended molecules, in sharp contrast with the spatially homogeneous electric fields of molecular spectroscopy.

Acknowledgements Work in Parma is supported by Italian MIUR through FIRB-RBNE01P4JF and PRIN2004033197–002. Work at Princeton is supported in part by the Princeton Research Institute on the Science and Technology of Materials (PRISM).

References

1. Mukamel S (1999) Principles of nonlinear optical spectroscopy. vol. 1 Oxford University Press
2. Katan C, Terenziani F, Mongin O, Werts MHV, Porrès L, Pons T, Mertz J, Tretiak S, Blanchard-Desce M (2005) J Phys Chem A 109:3024

3. Painelli A, Terenziani F In: Papadopoulos MG, Leszczynski J, Sadlej AJ (ed) Nonlinear optical properties of matter: from molecules to condensed phases,vol. 1. Kluwer (and references therein).
4. Girlando A, Painelli A, Bewick SA, Soos ZG (2004) Synth Met 141:129
5. Joachim C, Ratner MA (2005) PNAS 102:8800
6. Mulliken RS (1969) J Am Chem Soc 74:811
7. Mulliken RS, Person WB (1969) Molecular complexes: a lecture and reprint volume. vol. 1. Wiley, New York
8. Painelli A (1998) Chem Phys Lett 285, 352 (and references therein)
9. Del Freo L, Terenziani F, Painelli A (2002) J Chem Phys 116: 755
10. Painelli A (1999) Chem Phys 245:185
11. Boldrini B, Cavalli E, Painelli A, Terenziani F (2002) J Phys Chem A 106:6286: Terenziani F, Painelli A, Comoretto D (2000) J Phys Chem A 104:11049
12. Terenziani F, Painelli A, Katan C, Charlot M, Blanchard-Desce M (2006) J Am Chem Soc 128:15742
13. Woo HY, Liu B, Kohler B, Korystov D, Mikhailovsky A, Bazan GC (2005 J Am Chem Soc 127:14721
14. Le Droumaguet C, Mongin O, Werts MHV, Blanchard-Desce M (2005) Chem Commun 2802
15. Strehmel B, Sarker AM, Detert H (2003)Chem Phys Chem 4:249
16. Zhang Q, Silbey R (1990) J Chem Phys 92:4899
17. Ferretti A, Improta R, Lami A, Villani G (2000) J Phys Chem A 104:9591
18. Prassides K, Schatz PN, Wong KY, Day P (1996) J Phys Chem B 90:5588
19. Borghi GP, Girlando A, Painelli A, Voit J (1996) Europhys Lett 34:127
20. Onsager L (1936) J Am Chem Soc 58:1486
21. Reichardt C (1994) Chem Rev 94:2319
22. Detert H, Sugiono E, Kruse G (2002) J Phys Org Chem 15:638
23. Detert H, Schmitt V (2004) J Phys Org Chem 17:1051
24. Zhao W, Hou YJ, Wang XS, Zhang BW, Cao Y, Yang R, Wang WB, Xiao XR (1999) Sol Energy Mater Sol Cells 58:173
25. Dirk CW, Herndon WC, Cervantes-Lee F, Selnau H, Martinez S, Kalamegham P, Tan A, Campos G, Velez M, Zyss J, Ledoux I, Chengg L-T (1995) J Am Chem Soc 117:2214
26. Das S, Thomas KG, Ramanathan R, George MV, Kamat PV (1993) J Phys Chem 97:13625
27. Gude C, Rettig W (2000) J Phys Chem A 104:8050
28. Franco I, Tretiak S (2004) J Am Chem Soc 126:12130
29. Tretiak S, Saxena A, Martin RL, Bishop AR (2002) Phys Rev Lett 89:097402
30. Thompson AL, Gaab KM, Xu J, Bardeen CJ, Martínez TJ (2004) J Phys Chem A 108:671
31. Gaab KM, Thompson AL, Xu J, Martínez TJ, Bardeen CJ (2003) J Am Chem Soc 125:9288
32. Lahankar SA, West R, Varnavski O, Xie X, Goodson III T (2004) J Chem Phys 120:337
33. Goodson III TG (2005) Acc Chem Res 38:99
34. Varnavski OP, Ostrowski JC, Sukhomlinova L, Twieg RJ, Bazan GC, Goodson III T (2002) J Am Chem Soc 124:1736
35. Painelli A, Terenziani F (2000) J Phys Chem A 104:11041
36. Terenziani F, Painelli A, Girlando A, Metzger RM (2004) J Phys Chem B 108:10743
37. Terenziani F, Painelli A (2005) J Lumin 112:474
38. Painelli A, Terenziani F, Angiolini L, Benelli T, Giorgini L (2005) Chem Eur J 11:6053
39. Terenziani F, Painelli A (2003) Phys Rev B 68:165405
40. Painelli A, Terenziani F (2003) J Am Chem Soc 125:5624
41. Knoester J (2002)In: Agranovich VM, La Rocca GC (ed) Proceedings of the international school of physics "Enrico Fermi" 2001, Course CXLIX, organic nanostructures: science and applications,Vol. 1. p 149 IOS Press The Netherlands,
42. Tributsch H, Pohlmann L (1998) Science 279:1891
43. Iwai S, Tanaka S, Fujinuma K, Kishida H, Okamoto H, Tokura Y (2002) Phys Rev Lett 88:057402
44. Champagne B, Bishop DM (2003) Adv Chem Phys 126:41
45. Soos ZG, Klein DJ (1976) In: Hannay NB (ed) Treatise on solid-state chemistry, vol. 3. p 679 Plenum Press: New York,
46. Bewick SA, Pascal RA, Ho DM, Soos ZG, Masino M, Girlando A (2005) J Chem Phys 122:024710
47. Horiuchi S, Okimoto Y, Kumai R, Tokura Y (2001) J Am Chem Soc 123:665
48. Horiuchi S, Okimoto Y, Kumai R, Tokura Y (2003) Science 299:229
49. Soos ZG, Keller HJ, Moroni W, Nothe D (1978) Ann NY Acad Sci. 313:442.
50. Anusooya-Pati Y, Soos ZG, Painelli A (2001) Phys Rev B 63:205118
51. Del Freo L, Painelli A, Soos ZG (2002) Phys Rev Lett 89:27402
52. Soos ZG, Bewick SA, Peri A, Painelli A (2004) J Chem Phys 120:6712
53. Girlando A, Painelli A (1986) Phys Rev B 34:2131
54. Painelli A, Girlando A (1988) Phys Rev B 37:5748
55. Bray JW, Interrante LV, Jacobs IS, Bonner JC (1983) In: Miller JS (ed) Extended linear chain compounds, vol. 3. p 353 Plenum Press: New York
56. Bishop DM (1998) Adv Chem Phys 104:1
57. Resta R (2002) J Phys Condens Matter 14:R625
58. Buttiker M (1985) Phys Rev B 32:1846
59. Landauer R (1957) IBM J Res Dev 1:223
60. Datta S (2004) Nanotechnology 15:S433
61. Kamenev A, Kohn W (2001) Phys Rev B 63:155304
62. Bokes P, Mera H, Godby RW (2005) Phys Rev B 72:165425
63. Das MP, Green F, Thakur JS (2004) cond-mat 0404412: Das MP, Green F (2003) J Phys Condens Matter 15:L687
64. Painelli A (2006) Phys Rev B 74:155305
65. Sols F (1991) Phys Rev Lett 67:2874
66. Burke K, Car R, Gebauer R (2005) Phys Rev Lett 94:146803
67. Magnus W, Schoenmaker W (2000) Phys Rev B 61:10883
68. Kosov DS (2004) J Chem Phys 120:7165
69. Ng TK (1992) Phys Rev Lett 68:1018
70. Aviram A, Ratner MA (1974) Chem Phys Lett 29:274
71. Troisi A, Ratner MA (2002) J Am Chem Soc 124:14528
72. Berman O, Mukamel S (2004) Phys Rev B 69:155430
73. Levine IN (1991) Quantum chemistry, vol. 1. Prentice-Hall